Prion Diseases: Dynamics of the Infection and Properties of the Bistable Transition

Nicolas Kellershohn and Michel Laurent
Imagerie et Dynamique Cellulaires, UPRESA CNRS 8080, Université Paris-Sud, 91 405 Orsay Cedex, France

ABSTRACT Prion diseases are thought to result from a pathogenic, conformational change in a cellular protein, the prion protein. The pathogenic isoform seems to convert the normal isoform in an autocatalytic process. In contrast to the conditions used for in vitro studies of enzyme kinetics, the concentration of the catalyst is not much lower than that of the substrate in the course of infection. This feature may endow the system with a time-hierarchy allowing the pathogenic isoform to relax very slowly in the course of infection. This may contribute to the long incubation periods observed in prion diseases. The dynamic process of prion propagation, including turnover of the cellular prion protein, displays bistable properties. Sporadic prion diseases may result from a change in one of the parameters associated with metabolism of the prion protein. The bistable transition observed in sporadic disease is reversible, whereas that observed in cases of exogenous contamination is irreversible. This model is consistent with the occurrence of rare, sporadic forms of prion diseases. It may also explain why only some individuals of a cohort develop a prion disease following transient food contamination.

INTRODUCTION

There is compelling biochemical and genetic evidence (Prusiner, 1991; Bessen et al., 1995; Laurent and Johannin, 1997; Prusiner et al., 1998) to suggest that the agent responsible for the onset and propagation of transmissible spongiform encephalopathies (or prion diseases) is a pathogenic conformational isoform (PrP^{Sc}) of a protein encoded by a host gene (the prion protein, PrP^{C}). The pathogenic isoform is thought to multiply by converting the normal protein into a copy of itself in an autocatalytic process (Telling et al., 1996; Laurent, 1997). The frequency of spontaneous conversion of PrP^{C} into PrP^{Sc} is thought to be very low, accounting for the low incidence of sporadic prion diseases. However, inherited mutations in the Prp gene (leading to familial prion diseases) are likely to increase the frequency of the conversion, facilitating spontaneous expression of the disease within the lifetime of the individual.

Model studies (Laurent, 1996; Kacser and Small, 1996; Kepler, 1997; Porcher and Gatto, 2000) have shown that, in a physiological context including turnover of the normal isoform of the protein and its circulation through several cellular compartments, prion propagation corresponds to a switch between a normal and a pathogenic, alternative stable steady state (i.e., the system exhibits bistability). The dynamic component of mechanisms of protein conformational changes can help us to understand threshold properties of infection and contamination, the characteristics of interspecies transmission of prion diseases or the existence of a species barrier (Laurent, 1998; Kellershohn and Laurent, 1998). However, in all the models studied to date, phenomenological rate laws (derived from enzymatic catalysis) have been used to express the kinetics of conversion of PrP^{C} into PrP^{Sc}. These rate laws are valid only in conditions in which the concentration of the catalyst is much lower than that of the substrate. Clearly, this is only likely to be the case during the initial period of prion infection. As the conversion process progresses, the ratio of pathogenic to normal forms of the prion protein increases and the PrP^{Sc} isoform soon becomes predominant.

Attempts have been made to deal with situations of this type for enzyme catalysis (Halfman and Marcus, 1982; Laurent and Kellershohn, 1984; Kellershohn and Laurent, 1985). This concentration effect has been shown to modify profoundly the co-operative properties of multimeric enzymes. This situation closely resembles that for prions, because several lines of evidence (Bellinger-Kawahara et al., 1988; Sklaviadis et al., 1989, 1992; Jarret and Lansbury, 1993; Come et al., 1993; Eigen, 1996; Kepler, 1997; Laurent, 1997) suggest that the conformational transition of the prion protein proceeds via multimeric assembly of the pathogenic isoform of protein. However, the prion transformation mechanism has specific features not found in chemical or enzymatic reactions: the product of the transformation is the catalyst itself. We therefore thought it is important to investigate the effects of a large concentration of catalyst on the dynamics of prion propagation.

We describe here a realistic, molecular prion model that retains all the bistable properties previously described in the simplest phenomenological models. However, this molecular approach revealed additional new features of prion propagation. First, we found that the all-or-nothing transition induced by input of the exogenous, pathogenic isoform of the prion protein (contamination) corresponded to an irreversible transition. Second, by considering realistic values of kinetic constants and parameters, we showed the existence of different time scales in the dynamics of prion propagation. This time-hierarchy provides a possible explanation as to how the mech-

Received for publication 17 April 2001 and in final form 14 August 2001.
Address reprint requests to Michel Laurent, Imagerie et Dynamique Cellulaires, UPRESA CNRS 8080, Université Paris-Sud, bât. 440, 91 405 ORSAY Cedex, France. Tel.: +33-169-15-6294; Fax: +33-169-15-4956; E-mail: michel.laurent@ibaic.u-psud.fr.

0006-3495/01/11/2517/13 $2.00

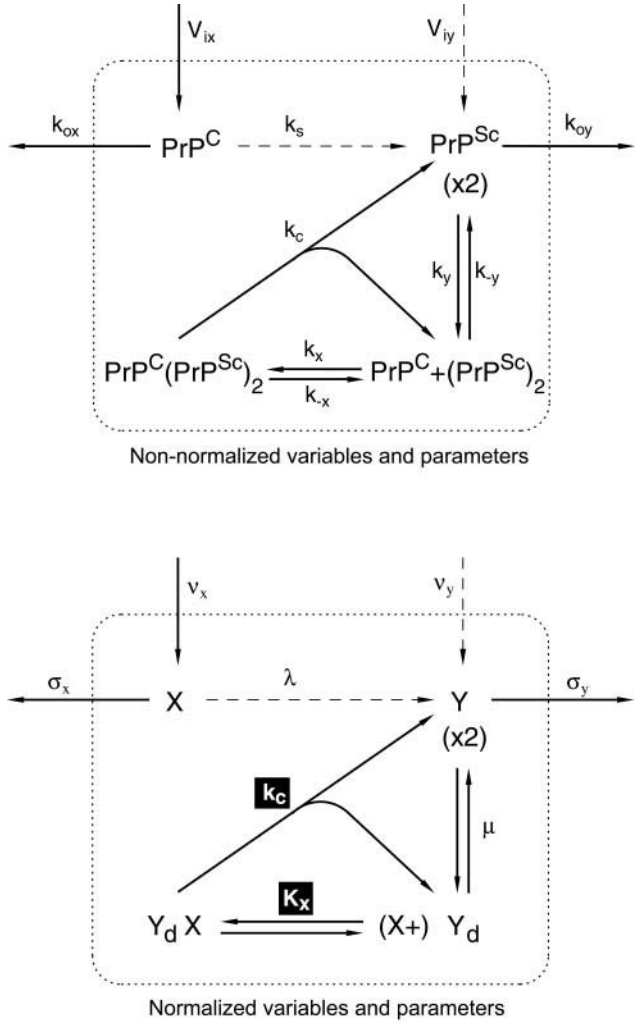

DIAGRAM 1.

anism of prion protein conversion contributes to the long incubation periods observed in prion diseases.

MODEL

Diagram 1 shows the overall mechanism suggested for prion propagation. X is PrP^C, the normal isoform of the prion protein, and Y represents the converted, pathogenic PrP^{Sc} species (Y and Y_d are the monomer and dimer forms of PrP^{Sc}, respectively). Conversion between the normal and pathogenic forms of the protein occurs via two different mechanisms: 1) A first-order reaction $\nu_s = k_s X$ corresponding to spontaneous conversion. The rate constant k_s is assumed to be very low, consistent with the observed low frequency of sporadic prion diseases. 2) An activated process of conformational change in which the homodimer Y_d is the effective catalyst. Conversion occurs via the formation of an intermediary complex Y_dX.

These reactions are thought to occur in an open system in which the X-species turns over (input rate ν_{ix} and first-order output rate $\nu_{ox} = k_{ox}X$). To make our model representative of several different situations, we considered the possible existence of an input flux ν_{iy} of the pathogenic species Y. A non-null value of ν_{iy} would mimic the occurrence of contamination. Amyloid plaques consisting of aggregates of the pathogenic isoform would then be formed through the ν_{oy} output process (first-order rate constant k_{oy}). Alternatively, this step may be associated with an unknown process of sequestration or the slow elimination of this pathogenic isoform.

Four- and two-variable systems

The changes in the concentrations of the species over time are described by four differential equations:

$$\frac{dX}{dt} = \nu_{ix} - (k_s + k_{ox})X - [k_x X \cdot Y_d - k_{-x} Y_d X] \quad (1a)$$

$$\frac{dY}{dt} = \nu_{iy} + k_s X + k_c Y_d X + 2[k_{-y} Y_d - k_y Y^2] - k_{oy} Y \quad (1b)$$

$$\frac{dY_d}{dt} = k_c Y_d X - [k_x X \cdot Y_d - k_{-x} Y_d X] - [k_{-y} Y_d - k_y Y^2] \quad (1c)$$

$$\frac{dY_d X}{dt} = [k_x X \cdot Y_d - k_{-x} Y_d X] - k_c Y_d X \quad (1d)$$

Due to the presence of the Y^2 and $X \cdot Y_d$ terms, these equations are nonlinear. Assuming rapid equilibrium both for the dimerization of Y (equilibrium constant $K_y = k_{-y}/k_y$) and for the binding of X on the Y_d species (equilibrium constant $K_x = k_{-x}/k_x$), this system reduces to a two-variable system. To reduce the number of parameters, dimensionless variables and parameters may be defined. We chose the following normalization:

$$x_T = \frac{X_T}{K_x}, \quad y_T = \frac{Y_T}{K_x}, \quad x = \frac{X}{K_x}, \quad y = \frac{Y}{K_x}, \quad y_d = \frac{Y_d}{K_x},$$
$$y_{dX} = \frac{Y_d X}{K_x}, \quad \tau = k_c t, \quad \lambda = \frac{k_s}{k_c}, \quad \sigma_x = \frac{k_{ox}}{k_c}, \quad (2)$$
$$\sigma_y = \frac{k_{oy}}{k_c}, \quad \mu = \frac{K_x}{K_y}, \quad \nu_x = \frac{\nu_{ix}}{k_c K_x}, \quad \nu_y = \frac{\nu_{iy}}{k_c K_x}$$

The equations of motion for the normalized, two-variable system are thus,

$$\frac{dx_T}{d\tau} = \nu_x - (\lambda + \sigma_x + \mu y^2)x = g_1(x, y),$$
$$\frac{dy_T}{d\tau} = \nu_y + (\lambda + \mu y^2)x - \sigma_y y = g_2(x, y), \quad (3)$$

with the two conservation equations:

$$x_T = x + \mu x y^2 = f_1(x, y),$$
$$y_T = y + 2\mu y^2(1 + x) = f_2(x, y). \quad (4)$$

The independent variables x_T and y_T represent the normalized, total (bound and unbound species) concentrations (expressed as monomer concentrations) of the normal and pathogenic forms of the prion protein, respectively. The numerical integration of Eq. 3 would require the solution, for each step of integration, of the system of nonlinear Eq. 4. For calculations, it is easier to consider x and y (the concentrations of the corresponding unbound species) as independent variables in place of x_T and y_T. We can write

$$\frac{dx_T}{d\tau} = \frac{\partial f_1}{\partial x}\frac{dx}{d\tau} + \frac{\partial f_1}{\partial y}\frac{dy}{d\tau}$$
$$= \nu_x - (\lambda + \sigma_x + \mu y^2)x = g_1(x, y),$$
$$\frac{dy_T}{d\tau} = \frac{\partial f_2}{\partial x}\frac{dx}{d\tau} + \frac{\partial f_2 dy}{\partial y d\tau} \quad (5)$$
$$= \nu_y + (\lambda + \mu y^2)x - \sigma_y y = g_2(x, y).$$

We can define vectors [U] and [G] and matrix [J] as

$$[U] = \begin{bmatrix} dx/d\tau \\ dy/d\tau \end{bmatrix}; \quad [G] = \begin{bmatrix} g_1 \\ g_2 \end{bmatrix};$$
$$[J] = \begin{bmatrix} j_{11} = 1 + \mu y^2 & j_{12} = 2\mu x y \\ j_{21} = 2\mu y^2 & j_{22} = 1 + 4\mu y(1 + x) \end{bmatrix}. \quad (6)$$

Because $[U] = [J]^{-1} \cdot [G]$, the differential system can be explicitly written as

$$\frac{dx}{d\tau} = \frac{j_{22}g_1 - j_{12}g_2}{j_{11}j_{22} - j_{12}j_{21}},$$
$$\frac{dy}{d\tau} = \frac{j_{11}g_2 - j_{21}g_1}{j_{11}j_{22} - j_{12}j_{21}}. \quad (7)$$

Numerical integrations of differential Eq. 7 were carried out with the Runge–Kutta fourth-order algorithm, with automatic step-size control and control of the relative error of integration at each step of the procedure.

Semi-parametric curves of steady states $h(y, p_k) = 0$ in the plane $[(\log)p_k, (\log)y_T]$

The equation $h(y, p_k) = 0$, where p_k represents any parameter of the model, may be obtained by eliminating the variable x between quasisteady-state equations $g_1(x, y) = 0$ and $g_2(x, y) = 0$, in which expressions for $g_1(x, y)$ and $g_2(x, y)$ are given in Eq. 3. We obtain

$$h(p_k, y) = (\nu_y - \sigma_y y)(\lambda + \sigma_x + \mu y^2) + \nu_x(\lambda + \mu y^2) = 0, \quad (8)$$

with the condition

$$\nu_y - \sigma_y y < 0 \Rightarrow y > \nu_y/\sigma_y. \quad (9)$$

The roots of Eq. 8 are obtained numerically.

RESULTS

Existence of multiple steady states in the prion system

The bistable characteristics of this prion model are shown in Fig. 1 *A*. Steady states are defined by constant values for the concentrations of the species. For the set of parameter values we used (and also over a wide range of other values), *X*- and *Y*-null isoclines have three intercepts, defining three steady states for the system. Normal mode analysis (Appendix A) demonstrates that any steady state (such as SS_2) corresponding to the part of the *Y*-null isocline that has a negative slope is unstable. Such steady states correspond to a saddle point (i.e., a simple threshold). Conversely, SS_1 and SS_3 are stable steady states and behave as attractors. SS_1 is associated with a low concentration y_T of the pathogenic isoform of the prion protein. It may be defined as a normal (nonpathogenic) state. Conversely, SS_3 corresponds to a high concentration (note the log scale in Fig. 1 *A*) y_T of the pathogenic prion protein *Y*. This steady state is a pathogenic state.

Figure 1 *A* also shows that the concentrations of unbound molecular species are significantly different from the total concentrations (bound and unbound) of the corresponding species. This difference seems to increase as the concentration of pathogenic isoforms increases: it is not significant in SS_1 and SS_2, whereas free and total concentrations are clearly different in the SS_3 steady state. For instance, the concentration of total, normal prion (x_T) is about ten thousand times higher than the free concentration of X (x) in the SS_3 steady state. In these conditions, autocatalytic conversion predominates over spontaneous conversion (or the process induced by the exogenous input of pathogenic species in contamination), resulting in a very high concentration of the ternary complex Y_dX (this concentration must be negligible in the classical formulation of enzyme catalysis). Thus, phenomenological rate equations derived from enzyme kinetics cannot be used to interpret prion behavior over the whole concentration range during infection and contamination.

Depending on the value of the input rate ν_x of the normal prion protein, the *X*- and *Y*-null isoclines have either one or three intercepts, and the system therefore has either one or three steady states (Fig. 1 *B*). Hence, the parameter dependence of the singularity or multiplicity of steady states must

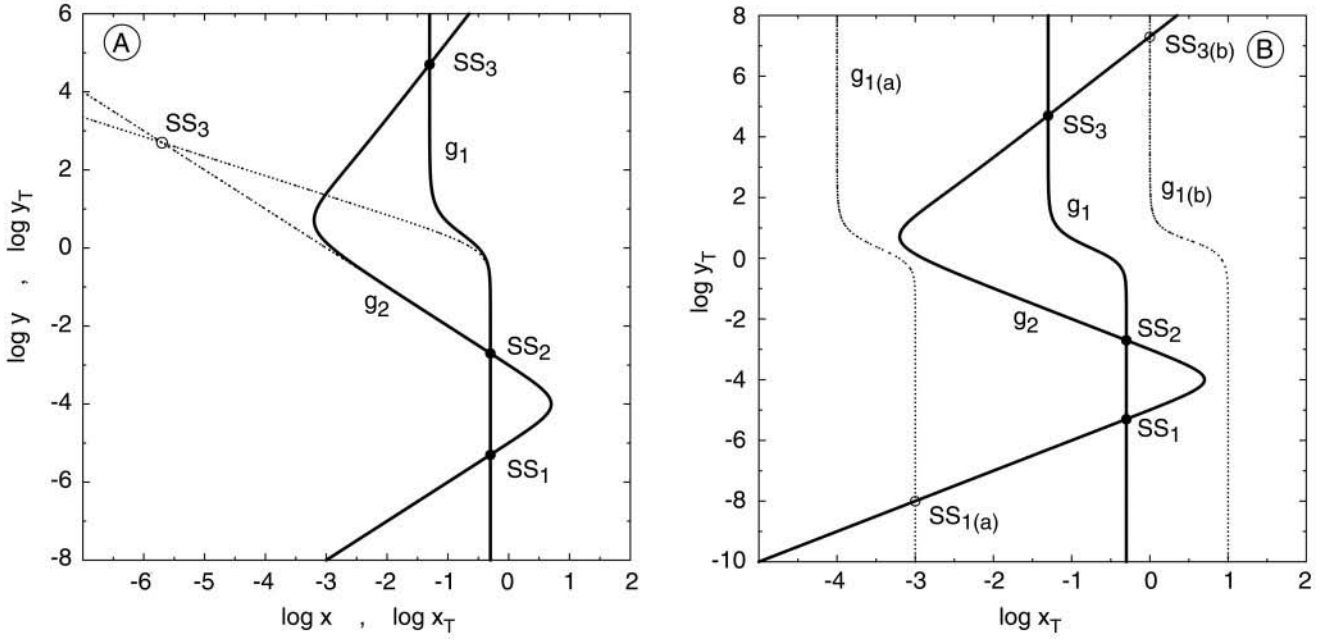

FIGURE 1 Phase plane analysis of the prion system showing the existence of multiple steady states. Curves show the quasi-steady-state lines (null isoclines) defined by equations $g_1(x, y) = 0$ and $g_2(x, y) = 0$. Expressions for $g_1(x, y)$ and $g_2(x, y)$ are given in Eq. 3. The corresponding equations were solved numerically. (*A*) The two null isoclines in the (log x_T, log y_T) plane (*thick lines*) or in the (log x, log y) plane (*thin lines*). Variables x_T and y_T correspond to the total (bound and unbound) concentration of the normal and pathogenic isoforms of the prion protein, respectively. Variables x and y represent the concentrations of the corresponding unbound isoforms. Free and total concentrations of the species appear quite different for high concentrations of the pathogenic isoform (in SS_3 steady state for instance), whereas they are not distinguishable for low values of y (as in SS_1 and SS_2 steady state for instance). (*B*) The singularity (*thin lines*) or multiplicity (*thick lines*) of steady states, according to the value of the input rate (ν_x) of the normal isoform of the prion protein. Note that the value of the input rate affects only the shape of the g_1 null-isocline, without modifying the shape or position of the g_2 null-isocline. A single, normal steady state $SS_{1(a)}$ exists for a low value of ν_x ($\nu_x = 10^{-4}$, null-isocline $g_{1(a)}$). A single but pathogenic steady state $SS_{3(b)}$ exists for a high value of ν_x ($\nu_x = 1$, null-isocline $g_{1(b)}$). For a medium value of the input rate ($\nu_x = 0.05$, g_1 null-isocline), three steady states, SS_1, SS_2 and SS_3, coexist. Curves were obtained with the following set of values: $\lambda = 10^{-9}$, $\sigma_x = 0.1$, $\sigma_y = 10^{-4}$, $\mu = 0.1$, $\nu_x = 0.05$, $\nu_y = 0$. We thus assume the absence of contamination due to the input of exogenous, pathogenic prion (ν_y parameter).

be considered with respect to the values of the main parameters of the model.

Sporadic diseases are associated with reversible, bistable transition

The semi-parametric curves in Fig. 2 show the dependence of the number and properties of the steady states of the system on several parameters. In each case, we observed the existence of a wide range (3–4 orders of magnitude) of values for which three (two stable and one unstable) steady states co-existed. For each of these parameters, there are two distinct limiting values beyond which the system possesses a single steady state. Beyond one of these values this single steady state corresponds to a normal (nonpathogenic) steady state because the concentration y_T of the pathogenic prion species is low. Beyond the other limiting value the steady state corresponds to a pathogenic steady state in which the concentration y_T of the pathogenic isoform is high.

As shown in Appendix B, explicit parametric conditions can be found for the existence of bistability in this model: $\sigma_x > 8\lambda$ and $\nu_x \in [\nu_{xl}, \nu_{xu}]$ or $\sigma_{yl} < \sigma_y < \sigma_{yu}$ with limiting values ν_{xl}, ν_{xu}, σ_{yl}, and σ_{yu} as given in Appendix B; and $\mu > 27\lambda(\sigma_y/\nu_x)^2$ and $\sigma_{xl} < \sigma_x < \sigma_{xu}$ with limiting values σ_{xl} and σ_{xu} as given in Appendix B. Hence, in this model, the conditions for the possible existence of several steady states do not depend on the efficiency of the catalyzed conversion. The condition $\sigma_x > 8\lambda$ seems to be satisfied in all cases. Thus, the rate of degradation (σ_x) of the normal prion protein must be eight times higher than the rate of spontaneous conversion of X into Y (λ). Indeed, the spontaneous conversion associated with the rare instances of sporadic disease is known to be a very slow process (annual background death rate of 0.5–1.5 per million for Creutzfeldt–Jakob Disease). In contrast, the normal prion protein is degraded rapidly, with an estimated half-life of 1 h (Borchelt et al., 1990).

The parametric conditions for the μ value are easily satisfied if $\mu < 1$ (Fig. 2 *C*), i.e., if the affinity of the pathogenic dimer Y_d for the normal species X is higher than that of the pathogenic monomer for itself (Y_d formation). In such conditions, the bistability domain corresponds to about six orders of magnitude of possible μ values. Conversely,

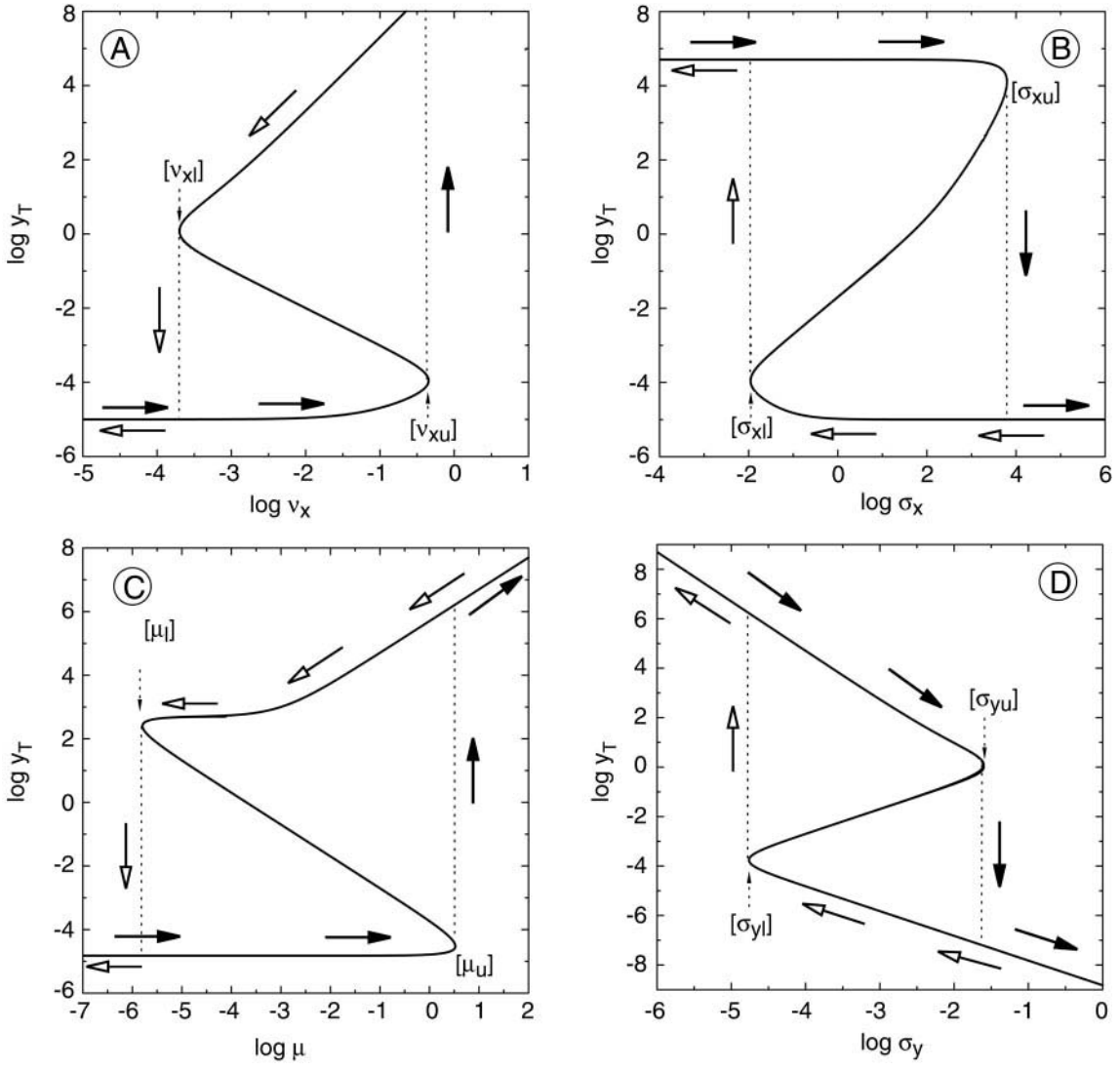

FIGURE 2 Trajectories of y_T steady states in several semiparametric planes. Reversibility of the bistable transition. The variable is the input rate ν_x of the normal isoform of the prion protein (*A*), the output rate σ_x of this normal isoform (*B*), the ratio μ of equilibrium constants for the dimerization of the pathogenic isoform and for the formation of the ternary, heterologous complex (*C*) or the output rate σ_y for elimination of the pathogenic isoform (*D*). In each case, the domain of bistability is limited by two distinct threshold values of the variable (see Appendix B). Upon increase (*black arrows*) or decrease (*white arrows*) of the variable, the system undergoes a transition from one stable solution to the other (*vertical dashed lines*). The lower steady-state branch corresponds to the normal steady state because it is associated with low values of the total concentration y_T of the pathogenic isoform of the prion protein. The upper branch of the trajectory is associated with high concentrations of *Y* isoform and corresponds to pathogenic steady states. The jump-like transitions between normal and pathogenic steady states occur at different threshold values of the variable, according to the direction of movement along the trajectory. This is typical of reversible, hysteretic bistable behavior. Curves were calculated with the following set of values of the parameters (standard values, except for the variable tested): $\lambda = 10^{-9}$, $\sigma_x = 0.1$, $\sigma_y = 10^{-4}$, $\mu = 0.1$, $\nu_x = 0.05$, $\nu_y = 10^{-9}$.

the range of the bistability domain is less than one order of magnitude for μ values if we assume that the equilibrium constants for the two types of multimeric assembly are inversely related.

As an example, we will describe the rationale and properties of this system for variations in the input rate ν_x of the normal prion protein. Let us assume that the system is initially in the normal SS_1 steady state and that a continuous increase in the input rate ν_x occurs (Fig. 2 *A*, *closed arrows*). Provided that ν_x does not exceed the limiting value ν_{xu}, y_T (and also x_T), concentrations are slightly readjusted to remain constant, consistent with the curve forming the trajectory of steady states. However, if ν_x exceeds the threshold ν_{xu}, the system moves to the SS_3 domain of stability, in which there is a high concentration y_T of the pathogenic species. This results in the appearance of a strong discontinuity for the transition between the normal and pathogenic steady states following a continuous in-

crease in the value of ν_x. Let us now assume that the system is initially in a pathogenic steady state, with a high ν_x value, and that a continuous decrease in the input rate ν_x occurs (Fig. 2 *A*, *open arrows*). A switch is observed between the pathogenic and normal states, but the "jump-like" transition occurs at a lower threshold value (ν_{xl}) than that which triggered the forward transition. Hence, the threshold values of ν_x are different for the forward and backward switches between the normal and pathogenic steady states. These threshold effects and hysteretic behavior are typical of the bistable properties of the prion system.

Similar behavior is observed upon variation of the σ_x, μ, and σ_y parameters (Fig. 2, *B* to *D*, respectively). This enables us to propose a possible, simple explanation for the occurrence of sporadic prion diseases. Such diseases probably correspond to: a change in the turnover rate for the normal prion protein (ν_x or σ_x parameters), a decrease in the rate of elimination of the pathogenic isoform of the protein (σ_y parameter), or a change in the binding constants associated with dimerization of the pathogenic isoform or the equilibrium constant associated with the interaction between the pathogenic dimer and the normal isoform of the prion protein (μ parameter). The last two possibilities imply that the definition of a healthy organism requires clarification. It is currently thought that a healthy organism possesses no molecules of the pathogenic isoform of the prion protein and that a single molecule would suffice to propagate the infection. Dynamics show that a healthy organism need not necessarily have a null concentration of the pathogenic isoform, but only a low concentration of this species, below the lower threshold.

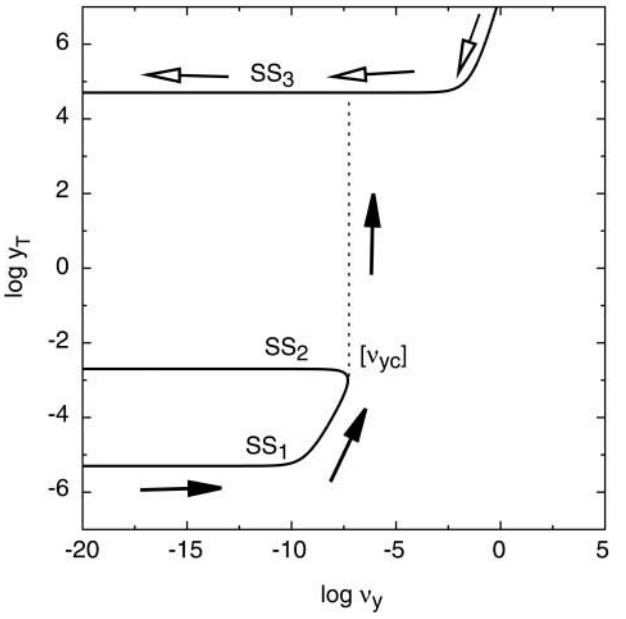

FIGURE 3 Trajectories of y_T steady states when the input rate ν_y of the exogenous, pathogenic isoform is the variable. Irreversibility of the bistable transition induced by a contamination process. When ν_y is the variable, the pathogenic, SS_3 steady-state branch corresponding to high y_T-concentrations of the pathogenic isoforms is not connected to the lower branch of stability corresponding to normal, SS_1 stable steady states. The lower threshold value of ν_y does not exist. Hence, increasing the input rate ν_y facilitates the jump-like transition from the normal to the pathogenic steady state (*black arrows*) but decreases (*white arrows*) in the value of this parameter (even to zero) do not provoke the reverse transition. The bistable transition that follows contamination is irreversible. The values of the parameters are as in Fig. 2.

Contamination results in irreversible transition

This prion model behaves differently if we assume that the disease results from an initial, exogenous supply (ν_y parameter) of the pathogenic isoform of the prion protein, as in contamination processes. The bifurcation diagram obtained if ν_y is the variable (Fig. 3) differs qualitatively from those of Fig. 2. The branch of steady states corresponding to high concentrations y_T of the pathogenic species is not connected to the lower branch of stability corresponding to normal, low y_T concentration. There is thus no lower limiting point corresponding to the threshold value (ν_{yl}) for the backward bistable transition.

If the system is in the normal SS_1 steady state and the input rate ν_y of exogenous, pathogenic prion protein increases such that it crosses the threshold ν_{yc}, the system will settle into the pathogenic SS_3 steady state (Fig. 3, *closed arrows*). However, if the perturbation is reversed (decrease in the value of ν_y), the system cannot switch back to the normal SS_1 steady state (Fig. 3, *open arrows*), even if ν_y reaches zero. The transition from the normal to the pathogenic steady state triggered by any contamination process is therefore irreversible.

Careful monitoring (data not shown) of the changes over time in concentration of all the molecular species and of the rate of each of the individual steps in Diagram 1 provides insight into the mechanism underlying this irreversible transition. If ν_y increases such that the concentration of the exogenous pathogenic isoform Y exceeds its threshold value, the concentration x of the unbound, normal isoform of the protein suddenly decreases. At the same time, there is a dramatic increase in the concentration y of the unbound, pathogenic isoform. This increase in y exceeds by several orders of magnitude the exogenous supply. It therefore corresponds to internal amplification of the perturbation. The system then slowly relaxes toward the stationary concentrations corresponding to the pathogenic SS_3 steady state. The concentrations of Y and Y_d isoforms are now so high that almost all the molecules of X are bound to form a binary or ternary complex with the pathogenic isoforms. In these conditions, Y production essentially results from the internal autocatalytic process of transformation and the contribution of the external supply of Y (ν_y) becomes negligible. This is why the transition cannot be reversed, even if $\nu_y = 0$.

Time hierarchy contributes to the duration of the incubation period in prion diseases

The mechanism of contamination by exogenous prion protein described above suggests that there is a time hierarchy in this model. This means that the system involves several simultaneous reactions that are not independent and that occur at very different rates.

Close to the normal SS_1 steady state, the concentrations of the binary Y_d and ternary Y_dX complexes are much lower than those of the unbound species, X and Y (Fig. 1 *A*). There is therefore no coupling of the metabolism of the normal X and pathogenic Y isoforms of the prion protein in the Y_dX complex in these conditions. Such metabolic coupling is ensured only by the spontaneous conversion of X into Y (λ parameter). However, this conversion is very slow (because the frequency of sporadic prion diseases is low). The unbound species X is therefore relaxed (i.e., its concentration is in a quasi-steady state) whereas the concentration of Y has not yet stabilized. In these conditions, the differential system of nonlinear Eq. 7 may be approximated by a system of two independent, linear differential equations,

$$\frac{dx}{d\tau} = \nu_x - (\lambda + \sigma_x)x \approx \nu_x - \sigma_x x,$$
$$\frac{dy}{d\tau} = (\nu_y + \nu'_y) - \sigma_y y, \tag{10}$$

where $\lambda x_1^* = \nu'_y = cste$ (x_1^* is the x concentration in the new steady state). The solution of Eq. 10 is (starting from initial conditions $\tau = 0$, $x_{(0)} = x_0$, $y_{(0)} = y_0$):

$$x_{(\tau)} = \frac{\nu_x}{(\lambda + \sigma_x)}\left[1 - e^{-(\lambda+\sigma_x)\tau}\right] + x_0 e^{-(\lambda+\sigma_x)\tau},$$
$$y_{(\tau)} = \frac{(\nu_y + \nu'_y)}{\sigma_y}\left[1 - e^{-\sigma_y\tau}\right] + y_0 e^{-\sigma_y\tau}, \tag{11}$$

with stationary values,

$$x_1^* = \frac{\nu_x}{\lambda + \sigma_x} \approx \frac{\nu_x}{\sigma_x}, \quad y_1^* = \frac{\nu_y + \nu'_y}{\sigma_y}. \tag{12}$$

If the system is beyond the transition threshold or close to the SS_3 (pathogenic) steady state, differential Eqs. 3 remain coupled, but may be simplified as (see discussion above)

$$\frac{dx_T}{d\tau} = \nu_x - \mu x y^2 = g_1(x, y),$$
$$\frac{dy_T}{d\tau} = \mu x y^2 - \sigma_y y = g_2(x, y). \tag{13}$$

In the SS_3 steady state, we have

$$\nu_x = \mu x^* y^{*2} = \sigma_y y^*. \tag{14}$$

We checked that the simplified expressions gave the same patterns of change over time as were obtained with the unsimplified differential system, for the range over which they could be applied.

Figure 4 shows the changes in time of y_T concentration on two different time scales, after a transient, suprathreshold perturbation-induced bistable transition from the normal, SS_1 steady state to the pathogenic, SS_3 state. In the short term (*insert*), the Y species seemed to relax rapidly, i.e., their concentration rapidly adopted an apparent, quasi-steady state. However, on a longer time scale, we observed that the pathogenic species relaxed much more slowly to their true, final steady state.

The correspondence between dimensionless and real non-normalized parameters may be assessed by isolating the subsystem consisting purely of the biosynthesis and degradation processes involving the normal isoform X of the prion protein. In the absence of the pathogenic isoform Y, changes in this subsystem over time are described by the differential equation,

$$\frac{dx_1}{d\tau} = \nu_x - \sigma_x x_1. \tag{15}$$

If we assume that this subsystem is displaced from its steady state ($x_1^* = \nu_x/\sigma_x$) by a slight perturbation $\Delta x_1^{(0)}$, we can write

$$\frac{d}{d\tau}(x_1^* + \Delta x_{1(\tau)}) = \underbrace{\frac{dx_1^*}{d\tau}}_{=0} + \frac{d\Delta x_{1(\tau)}}{dt} \approx \underbrace{f_{1(x_1^*)}}_{=0} + \left[\frac{df_1}{dx_1}\right]^* \Delta x_{1(\tau)} \tag{16}$$

and then

$$\Delta x_{1(\tau)} = \Delta x_1^{(0)} e^{-\sigma_x \tau}. \tag{17}$$

The relaxation time τ_x is such that $\tau_x = 1/\sigma_x$, and so, $\tau_{1/2} = \tau_x \ln 2 = \ln 2/\sigma_x$. The value of σ_x used in our simulations ($\sigma_x = 0.1$) leads to $\tau_x = 10$ and $\tau_{1/2} \approx 6.93$ (in normalized time units). According to Borchelt et al. (1990), the experimental relaxation time of the normal isoform of the prion protein is close to 20 min. Hence, one unit of normalized time corresponds to approximately 2 min.

In these conditions, $\tau_{1/2}$ for the relaxation of the pathogenic species Y (Fig. 4) would correspond to one year. After 2.5 years, the concentration y_T of these species would be only 80% of their final, steady-state concentration. These calculations are approximate because the neurophysiological processes that follow the accumulation of the pathogenic isoform may cause an additional lag time. However, they demonstrate that a simple dynamic model, based only on the conversion of the normal to the pathogenic isoform of the prion protein, is sufficient to account for very slow changes (on the time scale of about a year) in the concentration of the molecular species. Such a time scale is consistent with the length of the incubation period observed in prion diseases.

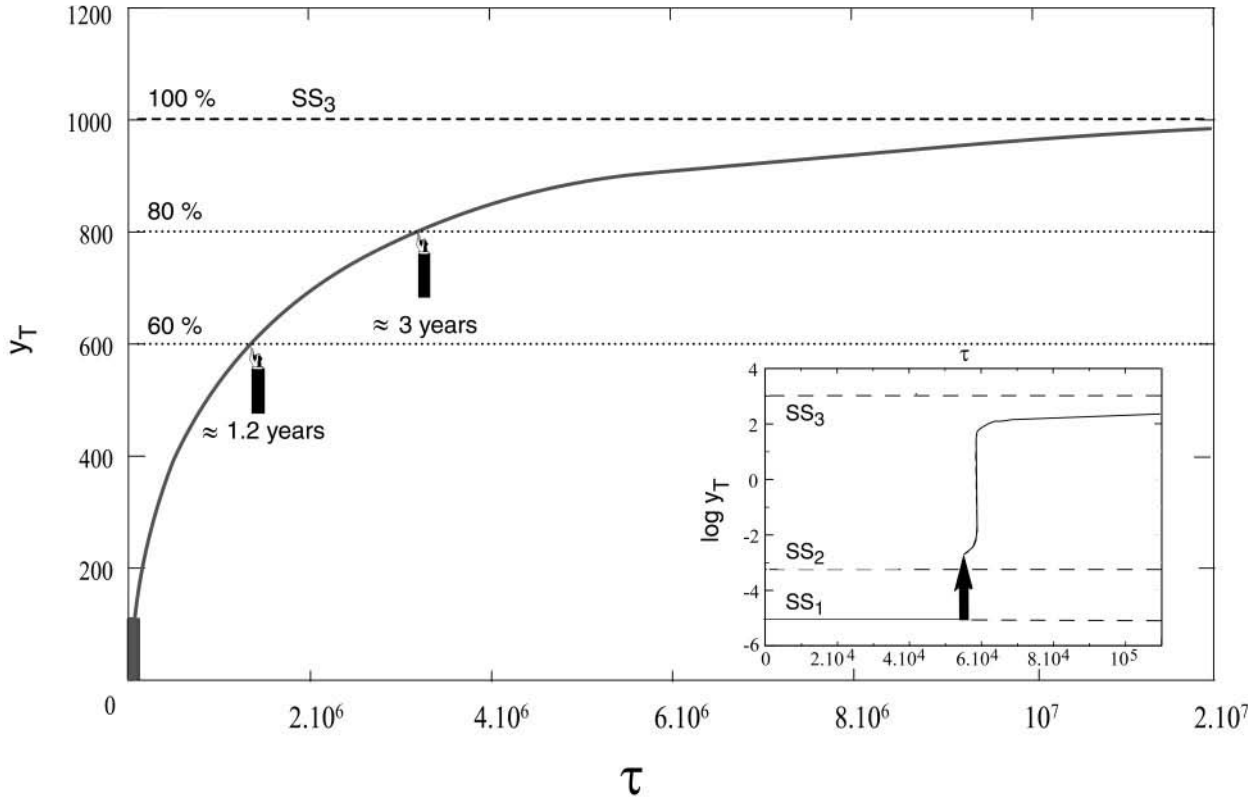

FIGURE 4 Long incubation periods in prion diseases due to a time hierarchy in the process of conversion of the protein. Initially ($\tau = 0$), the system is assumed to be in the normal steady state, SS_1, in which the concentration of the PrP^{Sc} isoform (y_T variable) is very low. The contamination process is simulated by adding a pulse of PrP^{Sc} beyond the SS_2 threshold (*insert*, *black arrow*). The form of the perturbation (continuous or instantaneous) and time for which it is applied would have no effect. The possible occurrence of the bistable transition depends only on the nature of the perturbation below or above the SS_2 threshold. Immediately after a suprathreshold perturbation, y_T-concentration increases markedly (*insert*), due to amplification of the pulse. In the short term (*insert*), the concentration of the *Y* species seems to arrive rapidly at a quasi-stationary value. However, this value corresponds to only ~10% of that in the final, SS_3 steady state (note the log scale in the insert). If the variation of y_T-concentration is observed over a longer time scale (*main figure*), it becomes apparent that this variable relaxes slowly toward the SS_3 steady state. The gray box near $\tau = 0$ in the main figure illustrates the extent of the scale used in the insert in *x* and *y* coordinates. The basis of the setting of the correspondence between dimensionless (τ) and real time units is described in the text. Curves were calculated (using the standard values of the parameters given in Fig. 2) by numerical integration of simplified Eq. 10 (*insert*) or 13 (*main Figure*). No difference would be observed in these changes over time if the complete system of Eq. 7 was used on both time scales.

DISCUSSION

The infectiousness of scrapie has been shown to be independent of the structures required for amyloid formation (Wile et al., 2000). However, models of infection based on a small, finite size of the catalytic PrP^{Sc} oligomer are often thought to be less likely to reflect the reality than nucleated polymerization models (Harper and Lansbury, 1997; Serio et al., 2000; Masel et al., 1999). This is because small finite-size models do not adequately account for the long incubation periods observed (Porcher and Gatto, 2000). In this study, we considered an oligomer-based model of this type brought close to physiological conditions, in which the concentrations of bound and unbound molecular species were clearly distinguished. We have shown that, in these conditions, the pathogenic isoform of the prion protein may relax very slowly over a time scale consistent with the incubation periods observed in animals. Death generally occurs soon after the onset of the disease, which occurs in the late stages of PrP^{Sc} accumulation (Beringue et al., 2000). Hence, the long incubation times of prion diseases, corresponding to years or even decades, may be at least partly related to the slow rate of an elementary step in the physicochemical conversion of the prion protein. However, these long incubation periods may result from complex biology rather than elementary, physicochemical processes.

This dynamic analysis suggests a possible mechanism for sporadic prion diseases and for certain specific features observed on contamination. In the proposed model, sporadic prion diseases correspond to changes in the rate of turnover of the normal isoform of the protein or, alternatively, in one of the parameters associated with metabolism of the pathogenic isoform. In accordance with this mechanism, it was shown that mice expressing high levels of PrP transgenes develop neural disorders (Westaway et al., 1994). The fre-

quency of the [URE3] phenotype (a yeast prion) is increased by overexpressing the URE2 gene and also by creating a mutant of the Ure2 protein (Fernandez-Bellot et al., 2000). One consequence of bistability is the absence of a snowball effect in the autocatalytic propagation of the pathogenic isoform provided that the concentration of both the pathogenic and normal isoforms remain below a certain threshold. It was experimentally shown that cell lines producing low steady-state levels of PrP^{C} protein were unable to propagate prions in transgenic mice (Korth et al., 2000). Consistent with our model, Manuelidis and Manuelidis (1993) reported the prevalence of small amounts of the pathogenic isoform of the prion protein in human lymphocytes. Immunohistochemical staining recently revealed the presence of the pathogenic isoform of the prion protein in the brains, nictitating membranes, and tonsils of two of seven healthy sheep (Kim et al., 2001). This raised the hope that such an immunohistochemical technique could be used for the early diagnosis of scrapie infection in sheep before the appearance of clinical signs. The results of our analysis do not support this view because they indicate that healthy organisms are not necessarily totally free of the pathogenic isoform. Thus, the presence of a small amount of the PrP^{Sc} isoform does not necessarily indicate an asymptomatic but infectious pathogenic state. This is also consistent with the recent proposal of Prusiner's group that the normal, native state of the prion protein may be marginally stable or unstable (Harrison et al., 2001). However, in the absence of amenable experimental data, we cannot give a quantitative estimate of the nonpathogenic, basic level of PrP^{Sc} isoform that might be present in the normal steady state.

From an experimental point of view, observation of distinct threshold values upon continuous forward and backward variations of a control parameter is the best test to demonstrate the existence of a reversible bistable transition (Laurent and Kellershohn, 1999). Such an experiment may be performed on the cellular [URE3] prion-like system, by modifying the controlled expression of the URE2 gene. Development of a permanent cell line supporting propagation of prion diseases is a prerequisite to develop such an experiment in the case of the prion protein. A recent report on a rabbit epithelial cell line (Vilette et al., 2001) seems to open up a promising avenue for such an approach.

Our results also relate to contamination processes. Although little is known about the precise mechanisms by which flocks and herds become contaminated with pathogenic prions, it is widely accepted that the ingestion of contaminated food is a major route of dissemination of prion diseases. Indeed, the rationale behind the policy of killing the entire herd if one cow is found to be contaminated with the agent of bovine spongiform encephalopathy (BSE) is that all the animals received the same food. However, clinical signs of the disease are generally detected in only one animal, or at most a small number of animals. Our model suggests a possible explanation for this surprising observation. The animals of the herd may differ in the parameters relating to metabolism of the prion protein. Most of the animals would be able to eliminate spontaneously amounts of the pathogenic isoform below the threshold ingested with their food, returning to the normal steady state after contamination. However, for some individuals with slight differences in prion metabolism, the same amount of contamination might be sufficient to reach the threshold and to provoke the disease. Typical populations of sheep seem to be closer to the threshold for pathogenic transition than typical populations of cows, because 10 to 15% of sheep in scrapie-infected flocks are often found to be contaminated, whereas the proportion of BSE-contaminated animals is generally much lower in cows.

At the population level, sporadic prion diseases and contamination processes are likely to share a number of important features. In all cases, the number of individuals that develop the disease depends on the heterogeneity of the population for the parameters relating to metabolism of the prion protein and the extent to which the mean value for these parameters deviates from the corresponding threshold value. However, other features differentiate sporadic diseases from contamination processes. Sporadic Creutzfeldt–Jakob Disease and the form resulting from transmission of the BSE agent to humans (new-Creutzfeldt–Jakob Disease) can be distinguished at the molecular level. We have previously shown (Laurent, 1998; Kellershohn and Laurent, 1998) that conformational adaptation of the prion protein may, in a bistability context, account for the main characteristics of this species barrier. In this paper, we also show that the bistable process observed upon contamination (input of exogenous, pathogenic isoform of the prion protein) corresponds to an irreversible bistable transition, whereas sporadic disease corresponds to a reversible, hysteretic transition. How important is this difference?

Irreversible transitions between multiple steady states have been studied in a variety of biochemical systems (for a review, see Laurent and Kellershohn, 1999). In the context of prion diseases, it is important to define precisely how this transition is irreversible. A transition is irreversible if the system cannot switch back to its previous steady state when the perturbation is reversed. As illustrated here for variations of the input rate ν_y of the pathogenic isoform of the prion protein, this occurs if one stable steady-state branch is not connected to the other stable branch. In the specific model studied here, we have shown that irreversibility results in alternation upon transition between two processes: exogenous PrP^{Sc} supply and autocatalytic, internal PrP^{Sc} production. Even if the exogenous supply is stopped, there is no effect on internal production after the transition has occurred, rendering this transition irreversible. However, the system selects one mode of operation in an irreversible manner only for a given set of parameter values. In the context of prion diseases, there may be situations in which the system would return to a normal steady state after

contamination has occurred, by acting simultaneously on several variables and parameters. This would correspond, for instance, to "cure" experiments (essentially performed in prion-like systems such as the [URE3] nonchromosomal genetic element in yeast (Edskes et al., 1999)). In this system, not only is the external supply of pathogenic isoform stopped, but all existing pathogenic isoforms are also removed from the system. However, in the case of the prion protein itself, the possible reversion of the bistable transition does not necessarily imply that the neurophysiological disorders that occurred when the system was in its pathogenic steady state will also be reversed. The distinction between reversible and irreversible bistable transitions would become important if we could experimentally detect early stages of infection, before the occurrence of neurological disorders.

APPENDIX A

Normal mode analysis of differential Eq. 7

For a small perturbation (Δx, Δy) close to the stationary values x^* and y^* of system 7, we can write

$$\begin{bmatrix} \mathrm{d}(\Delta x)/\mathrm{d}\tau \\ \mathrm{d}(\Delta y)/\mathrm{d}\tau \end{bmatrix} = [\mathbf{B}]^* \begin{bmatrix} \Delta x \\ \Delta y \end{bmatrix}, \tag{A1}$$

where $[\mathbf{B}]^*$ is the Jacobi matrix associated with differential Eq. 7, in which the value of each element b_{ij}^* is calculated at steady state. We have:

$$\begin{aligned} \det(\mathbf{J})^* b_{11}^* &= j_{22}^* \left[\frac{\partial g_1}{\partial x}\right]^* - j_{12}^* \left[\frac{\partial g_2}{\partial x}\right]^*; \\ \det(\mathbf{J})^* b_{12}^* &= j_{22}^* \left[\frac{\partial g_1}{\partial y}\right]^* - j_{12}^* \left[\frac{\partial g_2}{\partial y}\right]^*; \\ \det(\mathbf{J})^* b_{21}^* &= j_{11}^* \left[\frac{\partial g_2}{\partial x}\right]^* - j_{21}^* \left[\frac{\partial g_1}{\partial x}\right]^*; \\ \det(\mathbf{J})^* b_{22}^* &= j_{11}^* \left[\frac{\partial g_2}{\partial y}\right]^* - j_{21}^* \left[\frac{\partial g_1}{\partial y}\right]^*; \end{aligned} \tag{A2}$$

with

$$\begin{cases} j_{11}^* = 1 + \mu y^{*2}; & j_{12}^* = 2\mu x^* y^*, \\ j_{21}^* = 2\mu y^{*2}; & j_{22}^* = 1 + 4\mu y^*(1 + x^*), \end{cases} \tag{A3}$$

and

$$\begin{cases} [\partial g_1/\partial x]^* = -(\lambda + \sigma_x + \mu y^{*2}); \\ [\partial g_1/\partial y]^* = -2\mu x^* y^*, \\ [\partial g_2/\partial x]^* = \lambda + \mu y^{*2}; \\ [\partial g_2/\partial y]^* = 2\mu x^* y^* - \sigma_y. \end{cases} \tag{A4}$$

The eigenvalues of the Jacobi matrix are determined by the characteristic equation

$$\begin{aligned} r^2 - (b_{11}^* + b_{22}^*)r + (b_{11}^* b_{22}^* - b_{12}^* b_{21}^*) \\ = r^2 - \mathrm{tr}(\mathbf{B})^* r + \det(\mathbf{B})^* = 0, \end{aligned} \tag{A5}$$

where $\mathrm{tr}(\mathbf{B})$ is the trace and $\det(\mathbf{B})$ the determinant of the Jacobi matrix. It follows from Eq. A5 that the signs of the eigenvalues, and therefore the stability behavior of the system, are defined uniquely by the two terms $\mathrm{tr}(\mathbf{B})$ and $\det(\mathbf{B})$, which are complex functions of kinetic parameters.

Determinant $\det(\mathbf{B})^* = b_{11}^* b_{22}^* - b_{12}^* b_{21}^*$ of the Jacobi-matrix

According to Eq. A2, we can write

$$\begin{aligned} \det^2(\mathbf{J})^* \cdot \det(\mathbf{B})^* = &\left[j_{22}^* \left[\frac{\partial g_1}{\partial x}\right]^* - j_{12}^* \left[\frac{\partial g_2}{\partial x}\right]^* \right] \\ &\cdot \left[j_{11}^* \left[\frac{\partial g_2}{\partial y}\right]^* - j_{21}^* \left[\frac{\partial g_1}{\partial y}\right]^* \right] \\ &- \left[j_{22}^* \left[\frac{\partial g_1}{\partial y}\right]^* - j_{12}^* \left[\frac{\partial g_2}{\partial y}\right]^* \right] \\ &\cdot \left[j_{11}^* \left[\frac{\partial g_2}{\partial x}\right]^* - j_{21}^* \left[\frac{\partial g_1}{\partial x}\right]^* \right], \end{aligned} \tag{A6}$$

which leads to

$$\begin{aligned} \det^2(\mathbf{J})^* \cdot \det(\mathbf{B})^* = &\underbrace{(j_{11}^* j_{22}^* - j_{12}^* j_{21}^*)}_{\det(\mathbf{J})^*} \left[\frac{\partial g_1}{\partial x}\right]^* \left[\frac{\partial g_2}{\partial y}\right]^* \\ &- \underbrace{(j_{11}^* j_{22}^* - j_{12}^* j_{21}^*)}_{\det(\mathbf{J})^*} \left[\frac{\partial g_1}{\partial y}\right]^* \left[\frac{\partial g_2}{\partial x}\right]^*, \end{aligned} \tag{A7}$$

and then

$$\det(\mathbf{J})^* \cdot \det(\mathbf{B})^* = \left[\frac{\partial g_1}{\partial x}\right]^* \left[\frac{\partial g_2}{\partial y}\right]^* - \left[\frac{\partial g_1}{\partial y}\right]^* \left[\frac{\partial g_2}{\partial x}\right]^*. \tag{A8}$$

Every partial derivative in Eq. A8 may be expressed as a function of y^* as a single variable (taking into account the relationship between stationary x^* and y^* values). Thus,

$$\begin{aligned} \det(\mathbf{J})^* \cdot \det(\mathbf{B})^* = (\lambda + \mu y^{*2}) \Bigg\{ \sigma_y \left[1 + \frac{\sigma_x}{\lambda + \mu y^{*2}} \right] \\ - \frac{2\sigma_x \mu y^*}{(\lambda + \mu y^{*2})^2} (\sigma_y y^* - \nu_y) \Bigg\}. \end{aligned} \tag{A9}$$

The expression denoted by $\{\cdots\}$ in the right-hand term of Eq. A9 corresponds to the stationary expression of the derivative $\mathrm{d}\nu_x/\mathrm{d}y$. Hence,

$$\det(\mathbf{J})^* \cdot \det(\mathbf{B})^* = (\lambda + \mu y^{*2}) \left[\frac{\mathrm{d}\nu_x}{\mathrm{d}y}\right]^*. \tag{A10}$$

Because

$$\begin{aligned} \det(\mathbf{J})^* &= j_{11}^* j_{22}^* - j_{12}^* j_{21}^* \\ &= (1 + \mu y^{*2})(1 + 4\mu y^*) + 4\mu x^* y^* > 0 \end{aligned} \tag{A11}$$

every stationary value, in the semi-parametric plane (ν_x, y) or ($\log \nu_x$, $\log y$), located in the region of negative slope of the trajectory of steady states, is associated with a negative value of the determinant of the Jacobi matrix. Conversely, the regions of positive slope of this curve are associated with $\det(\mathbf{B})^* > 0$.

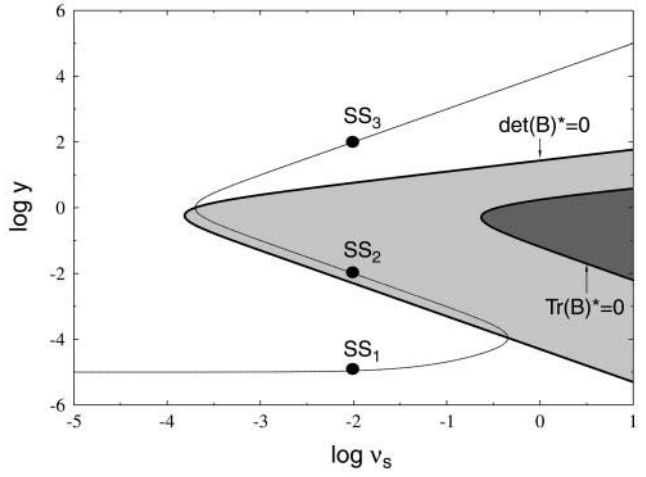

FIGURE 5 Parameter regions of the prion system represented in Diagram 1 with different stability properties. The trajectory of steady states and the curves tr(**B**)* = 0 and det(**B**)* = 0 obtained from normal mode analysis of differential Eq. 7 are represented in the (log y, log ν_x) semi-parametric plane. The SS_1 and SS_3 steady states both correspond to stable nodes because they are in the white region of the plane in which the trace of the Jacobi matrix is negative and its determinant is positive. Conversely, the SS_2 steady state is unstable: it corresponds to a saddle point because it lies in the light gray region of the plane in which both the determinant and the trace of the Jacobi matrix are negative. The dark gray region of the plane (in which there is no steady state) corresponds to an unstable node region (as we have tr(**B**)* > 0 and det(**B**)* > 0). Curves were calculated using the standard values of the parameters given in Fig. 2.

The condition det(**B**)* < 0 means that the roots r_1 and r_2 of the characteristic Eq. A5 do not have the same sign. Because, in these conditions, we also have $\mathrm{tr}^{*2}(\mathbf{B}) - 4\det(\mathbf{B})^* > 0$, these roots are necessarily real. We can conclude that any steady state for which det(**B**)* < 0 is an unstable steady state corresponding to a saddle point.

Trace tr(B)* = $b^*_{11} + b^*_{22}$ of the Jacobi matrix

Considering Eqs. A2–A4, we can write

$$\det(\mathbf{J})^* \cdot \mathrm{tr}(\mathbf{B})^* = j^*_{22}\left[\frac{\partial g_1}{\partial x}\right]^* - j^*_{12}\left[\frac{\partial g_2}{\partial x}\right]^* + j^*_{11}\left[\frac{\partial g_2}{\partial y}\right]^* - j^*_{21}\left[\frac{\partial g_1}{\partial y}\right]^*, \quad \text{(A12)}$$

which leads to

$$\begin{aligned}\det(\mathbf{J})^* \cdot \mathrm{tr}(\mathbf{B})^* &= -\sigma_x[1 + 4\mu y^*(1 + x^*)] \\ &\quad - (\lambda + \mu y^{*2})[1 + 2\mu y^*(1 + 3x^*)] \\ &\quad - \sigma_y(1 + \mu y^{*2}) \\ &\quad + \underbrace{2\mu x^* y^*(1 + 3\mu y^{*2})}_{>0}. \end{aligned} \quad \text{(A13)}$$

Eq. A13 indicates that the sign of the trace of the Jacobi matrix may change when the system moves from one steady state to another. The local stability of steady states in the (log ν_x, log y) semi-parametric plane is shown in Fig. 5, for a standard set of parameter values. In this plane, the trajectory of Y-steady states is represented, together with the lines tr(**B**)* = 0 and det(**B**)* = 0. These lines divide the plane into three domains (note that everywhere in this plane, the discriminant $\Delta^* = \mathrm{tr}^2(\mathbf{B}) - 4\det(\mathbf{B})^*$ is positive):

(1) tr(**B**)* < 0 and det(**B**)* > 0 Stable node
(2) tr(**B**)* < 0 and det(**B**)* < 0 Saddle point
(3) tr(**B**)* > 0 and det(**B**)* < 0 Saddle point

Stationary values of y^* in the region of positive slope of the curve $\log y^* = f(\log \nu_x)$ are located in domain (1). Hence, corresponding SS_1 and SS_3 steady states are locally stable. Conversely, stationary values of y^* in the region of negative slope of the curve $\log y^* = f(\log \nu_x)$ are located in domain (2). So, SS_2 steady states are locally instable and correspond to saddle points.

APPENDIX B

Parametric conditions for the coexistence of multiple steady states

The multiplicity of steady states in this model is associated with the S-shape of the graphs $\log y^*$ (or $\log y^*_T$) $= f(\log p_k)$ (in which p_k represents any of the ν_x, σ_x, σ_y, μ parameters). This S-shape is conserved in non-logarithmic coordinates. For each of these parameters, we can write an explicit function $F(\,)$ such as $p_k = F(y, p_{1\neq k})$. Hence, the condition for the coexistence of multiple steady states is equivalent to the condition for the existence of two real, positive roots for the equation $F'_{(y)} = 0$ (in which F' is the first derivative F with respect to y). Calculations were performed under the simplifying assumption $\nu_y = 0$ (absence of exogenous contamination). By eliminating variable x between null-isoclines $g_1(x, y) = 0$ and $g_2(x, y) = 0$ derived from Eq. 3, we obtain the polynomial equation,

$$\begin{aligned} h(y) &= \sigma_y y(\lambda + \sigma_x + \mu y^2) - \nu_x(\lambda + \mu y^2) \\ &= (\sigma_y y - \nu_x)(\lambda + \mu y^2) + \sigma_x\sigma_y y = 0 \end{aligned} \quad \text{(B1)}$$

with the condition

$$\sigma_y y - \nu_x < 0 \leftrightarrow y < \nu_x/\sigma_y. \quad \text{(B2)}$$

ν_x as a control parameter

We can write, from Eq. B1,

$$\begin{aligned} \nu_x = F(y) &= \sigma_y y \frac{\lambda + \sigma_x + \mu y^2}{\lambda + \mu y^2} \\ &= \sigma_y y\left[1 + \frac{\sigma_x}{\lambda + \mu y^2}\right], \end{aligned} \quad \text{(B3)}$$

and then

$$\frac{d\nu_x}{dy} = F'(y) = \sigma_y\left[1 + \frac{\sigma_x}{\lambda + \mu y^2} - \frac{2\sigma_x\mu y^2}{(\lambda + \mu y^2)^2}\right], \quad \text{(B4)}$$

$$F'(y) = 0 \Rightarrow (\mu y^2)^2 - (\sigma_x - 2\lambda)\mu y^2 + \lambda(\lambda + \sigma_x) = 0. \quad \text{(B5)}$$

The discriminant of Eq. B5 is positive when

$$\frac{\lambda}{\sigma_x} < \frac{1}{8}. \quad \text{(B6)}$$

The roots of Eq. B6 are

$$y_1 = \left[\frac{1}{2\mu}\left[\sigma_x - 2\lambda - \sqrt{\sigma_x(\sigma_x - 8\lambda)}\right]\right]^{1/2},$$

$$\text{and } y_2 = \left[\frac{1}{2\mu}\left[\sigma_x - 2\lambda + \sqrt{\sigma_x(\sigma_x - 8\lambda)}\right]\right]^{1/2}, \quad \text{(B7)}$$

with $y_2 > y_1 > 0$. The limit ν_x values are then

$$\nu_{xu} = \sigma_y y_1\left[1 + \frac{\sigma_x}{\lambda + \mu y_1^2}\right]$$

$$\text{and } \nu_{xl} = \sigma_y y_2\left[1 + \frac{\sigma_x}{\lambda + \mu y_2^2}\right]. \quad \text{(B8)}$$

Condition B6 is necessary for the existence of multiple steady states in this model. This condition becomes necessary and sufficient if we add the supplementary condition for ν_x,

$$\nu_x \in [\nu_{xl}, \nu_{xu}]. \quad \text{(B9)}$$

σ_x as a control parameter

We can write, from Eq. B1,

$$\sigma_x(y) = F(y) = (\lambda + \mu y^2)\left(\frac{\nu_x}{\sigma_y y} - 1\right), \quad \text{(B10)}$$

under the condition

$$y < \nu_x/\sigma_y. \quad \text{(B11)}$$

The derivative $F'(y)$ is

$$F'(y) = \frac{d\sigma_x}{dy} = \frac{1}{\sigma_y y^2}\left[\nu_x\mu y^2 - 2\sigma_y\mu y^3 - \lambda\nu_x\right]. \quad \text{(B12)}$$

y-values for which the derivative $F'(y)$ is null are the roots of the equation,

$$G(y) = 2\sigma_y\mu y^3 - \nu_x\mu y^2 + \lambda\nu_x = 0. \quad \text{(B13)}$$

Descartes' sign rule shows that Eq. B13 cannot have more than two real, positive roots for y. Taking into account the condition B11, graphical analytical evaluation of $G(y)$ shows that the condition for the existence of these two roots is

$$\mu > 27\lambda\left(\frac{\sigma_y}{\nu_x}\right)^2. \quad \text{(B14)}$$

The necessary and sufficient condition to obtain multiple steady states when σ_x is the control parameter, is expressed by Eq. B14 with the limiting values of σ_x such that

$$\sigma_{xl} < \sigma_x < \sigma_{xu}, \quad \text{(B15)}$$

with

$$\sigma_{xl} = \sigma_{x(y=y_1)} = (\lambda + \mu y_1^2)\left(\frac{\nu_x}{\sigma_y y_1} - 1\right)$$

$$\text{and } \sigma_{xu} = \sigma_{x(y=y_2)} = (\lambda + \mu y_2^2)\left(\frac{\nu_x}{\sigma_y y_2} - 1\right), \quad \text{(B16)}$$

where y_1 and y_2 are the two roots of Eq. B13.

σ_y as a control parameter

We can write, from Eq. B1,

$$\sigma_y(y) = F(y) = \frac{\nu_x(\lambda + \mu y^2)}{y(\lambda + \sigma_x + \mu y^2)}, \quad \text{(B17)}$$

and then

$$\frac{d\sigma_y}{dy} = F'(y)$$

$$= \nu_x\left[\frac{2\mu y^2(\lambda + \sigma_x + \mu y^2) - (\lambda + \mu y^2)[\lambda + \sigma_x + 3\mu y^2]}{y^2(\lambda + \sigma_x + \mu y^2)^2}\right]. \quad \text{(B18)}$$

The condition $F'(y) = 0$ leads to the same equation as does Eq. B5. Thus, the necessary and sufficient condition for the existence of multiple steady states when σ_y is the control parameter is expressed by Eq. B6 with the limiting values of σ_y, such that

$$\sigma_{yl} < \sigma_y < \sigma_{yu}, \quad \text{(B19)}$$

with

$$\sigma_{yl} = \sigma_y(y = y_1) = \frac{\nu_x(\lambda + \mu y_1^2)}{y_1(\lambda + \sigma_x + \mu y_1^2)}$$

$$\text{and } \sigma_{yu} = \sigma_y(y = y_2) = \frac{\nu_x(\lambda + \mu y_2^2)}{y_2(\lambda + \sigma_x + \mu y_2^2)}, \quad \text{(B20)}$$

in which expressions of y_1 and y_2 are given by Eq. B7.

μ as a control parameter

We can write, from Eq. B1,

$$\mu(y) = \frac{1}{y^2}\left[\frac{\sigma_x\sigma_y y}{\nu_x - \sigma_y y} - \lambda\right], \quad \text{(B21)}$$

and then

$$\frac{d\mu}{dy} = F'(y)$$

$$= \frac{2(\lambda + \sigma_x)(\sigma_y y)^2 - \nu_x(4\lambda + \sigma_x)(\sigma_y y) + 2\lambda\nu_x^2}{y^3(\nu_x - \sigma_y y)^2}. \quad \text{(B22)}$$

The condition for the existence of two real, positive roots for equation $F'(y) = 0$ is identical to the condition expressed in Eq. B5. Under this condition, the coordinates of the extremes for the $\mu(y)$ function are

$$y_1 = \frac{\nu_x}{4\sigma_y(\lambda + \sigma_x)}\left[4\lambda + \sigma_x - \sqrt{\sigma_x(\sigma_x - 8\lambda)}\right];$$

$$\mu_1 = \frac{1}{y_1^2}\left[\frac{\sigma_x\sigma_y y_1}{\nu_x - \sigma_y y_1} - \lambda\right];$$

$$y_2 = \frac{\nu_x}{4\sigma_y(\lambda + \sigma_x)}\left[4\lambda + \sigma_x + \sqrt{\sigma_x(\sigma_x - 8\lambda)}\right];$$

$$\mu_2 = \frac{1}{y_2^2}\left[\frac{\sigma_x\sigma_y y_2}{\nu_x - \sigma_y y_2} - \lambda\right]. \quad \text{(B23)}$$

This work was supported by grants from the Centre National de la Recherche Scientifique, the Université Paris-Sud, and the program Action Concertée Coordonnée "Epidémiologie des ESST".

REFERENCES

Bellinger-Kawahara, C. G., E. Kempner, D. F. Groth, R. Gabizon, and S. B. Prusiner. 1988. Scrapie prion liposomes and rods exhibit target sizes of 55,000 Da. *Virology.* 164:537–541.

Beringue, V., F. Lamoury, K. T. Adjou, T. Maignien, M. Demoy, P. Couvreur, and D. Dormont. 2000. Pharmacological manipulation of early PrPres accumulation in the spleen of scrapie-infected mice. *Arch. Virol. Suppl.* 16:39–56.

Bessen, R. A., D. A. Kocisko, G. J. Raymond, S. Nandan, P. T. Lansbury, and B. Caughey. 1995. Non-genetic propagation of strain-specific properties of scrapie prion protein. *Nature.* 375:698–700.

Borchelt, D. R., M. Scott, A. Taraboulos, N. Stahl, and S. B. Prusiner. 1990. Scrapie and cellular prion proteins differ in their kinetics of synthesis and topology in cultured cells. *J. Cell Biol.* 110:743–752.

Come, J. H., P. E. Fraser, and P. T. Lansbury. 1993. A kinetic model for amyloid formation in the prion diseases: importance of seeding. *Proc. Natl. Acad. Sci. U.S.A.* 90:5959–5963.

Edskes, H. K., V. T. Gray, and R. B. Wickner. 1999. The [URE3] prion is an aggregated form of Ure2p that can be cured by overexpression of Ure2p fragments. *Proc. Natl. Acad. Sci. U.S.A.* 96:1498–1503.

Eigen, M. 1996. Prionics or the kinetic basis of prion diseases. *Biophys. Chem.* 63:A1–A18.

Fernandez-Bellot, E., E. Guillemet, and C. Cullin. 2000. The yeast prion [URE3] can be greatly induced by a functional mutated URE2 allele. *EMBO J.* 19:3215–3222.

Halfman, C. J., and F. Marcus. 1982. A method for determining kinetic parameters at high enzyme concentrations. *Biochem. J.* 203:339–342.

Harper, J. D., and P. T. Lansbury. 1997. Models of amyloid seeding in Alzheimer's disease and scrapie: mechanistic truths and physiological consequences of the time-dependent solubility of amyloid proteins. *Annu. Rev. Biochem.* 66:385–407.

Harrison, P. M., H. S. Chan, S. B. Prusiner, and F. E. Cohen. 2001. Conformational propagation with prion-like characteristics in a simple model of protein folding. *Protein Sci.* 10:819–835.

Jarret, J. T., and P. T. Lansbury. 1993. Seeding "one-dimensional crystallization" of amyloid: a pathogenic mechanism in Alzheimer's disease and scrapie? *Cell.* 73:1055–1058.

Kacser, H., and J. R. Small. 1996. How many phenotypes from one genotype? The case of prion diseases. *J. Theoret. Biol.* 182:209–218.

Kellershohn, N., and M. Laurent. 1985. Analysis of progress curves for a highly concentrated Michaelian enzyme in the presence or absence of product inhibition. *Biochem. J.* 231:65–74.

Kellershohn, N., and M. Laurent. 1998. Species barrier in prion diseases: a kinetic interpretation based on the conformational adaptation of the prion protein. *Biochem. J.* 334:539–545.

Kepler, T. B. 1997. Oligomerization and Prp^{Sc} stability in prion propagation: a mathematical analysis. *In* Advances in Mathematical Population Dynamics: Molecules, Cells and Man. O. Arino, D. Axelrod and M. Kimmel editors. World Scientific, Singapore.

Kim, H., K. O'Rourke, M. Walter, H. G. Purchase, J. Enck, and T. K. Shin. 2001. Immunohistochemical detection of scrapie prion proteins in clinically normal sheep in Pennsylvania. *J. Vet. Diagn. Invest.* 13:89–91.

Korth, C., K. Kaneko, and S. B. Prusiner. 2000. Expression of unglycosylated mutated prion protein facilitates PrP^{Sc} formation in neuroblastoma cells infected with different prion strains. *J. Gen. Virol.* 81: 2555–2563.

Laurent, M. 1996. Prion diseases and the 'protein only' hypothesis: a theoretical dynamic study. *Biochem. J.* 318:35–39.

Laurent, M. 1997. Autocatalytic processes in cooperative mechanisms of prion diseases. *FEBS Lett.* 407:1–6.

Laurent, M. 1998. Bistability and the species barrier in prion diseases: stepping across the threshold or not. *Biophys. Chem.* 72:211–222.

Laurent, M. and G. Johannin. 1997. Molecular clues to pathogenesis in prion diseases. *Histol. Histopathol.* 12:583–594.

Laurent, M. and N. Kellershohn. 1984. Apparent cooperativity for highly concentrated Michaelian and allosteric enzymes. *J. Mol. Biol.* 174: 543–555.

Laurent, M. and N. Kellershohn. 1999. Multistability: a major means of differentiation and evolution in biological systems. *Trends Biochem. Sci.* 24:418–422.

Manuelidis, E. E. and L. Manuelidis. 1993. A transmissible Creutzfeldt–Jakob disease-like agent is prevalent in human populations. *Proc. Natl. Acad. Sci. U.S.A.* 90:7724–7728.

Masel, J., V. A. Jansen, and M. A. Nowak. 1999. Quantifying the kinetic parameters of prion replication. *Biophys. Chem.* 77:139–152.

Porcher, E. and M. Gatto. 2000. Quantifying the dynamics of prion infection: a bifurcation analysis of Laurent's model. *J. Theoret. Biol.* 205:283–296.

Prusiner, S. B. 1991. Molecular biology of prion diseases. *Science.* 252: 1515–1522.

Prusiner, S. B., M. R. Scott, S. J. DeArmond, and F. E. Cohen. 1998. Prion protein biology. *Cell.* 93:337–348.

Serio, T. R., A. G. Cashikar, A. S. Kowal, G. J. Sawicki, J. J. Moslehi, L. Serpell, M. F. Arnsdorf, and S. L. Lindquist. 2000. Nucleated conformational conversion and the replication of conformational information by a prion determinant. *Science.* 289:1317–1321.

Sklaviadis, T., R. Dreyer, and L. Manuelidis. 1992. Analysis of Creutzfeldt–Jakob disease infectious fractions by gel permeation chromatography and sedimentation field flow fractionation. *Virus. Res.* 26: 241–254.

Sklaviadis, T. K., L. Manuelidis, and E. E. Manuelidis. 1989. Physical properties of the Creutzfeldt–Jakob disease agent. *J. Virol.* 63: 1212–1222.

Telling, G. C., M. Parchi, S. J. DeArmond, P. Cortelli, P. Montagna, R. Gabizon, J. Mastrianni, E. Lugaresi, P. Gambetti, and S. B. Prusiner. 1996. Evidence for the conformation of the pathologic isoform of the prion protein enciphering and propagating prion diversity. *Science.* 274:2079–2082.

Vilette, D., O. Andreoletti, F. Archer, M. F. Madelaine, J. L. Volotte, S. Lehmann, and H. Laude. 2001. Ex vivo propagation of infectious sheep scrapie agent in heterologous epithelial cells expressing ovine prion protein. *Proc. Natl. Acad. Sci. U.S.A.* 98:4055–4059.

Westaway, D., S. J. DeArmond, C. J. Cayetano, D. Groth, D. Foster, S. L. Yang, M. Torchia, G. A. Carlson, and S. B. Prusiner. 1994. Degeneration of skeletal muscle, peripheral nerves, and the central nervous system in transgenic mice overexpressing wild-type prion proteins. *Cell.* 76: 117–129.

Wille, H., S. B. Prusiner, and F. Cohen. 2000. Scrapie infectivity is independent of amyloid staining properties of the N-terminally truncated prion protein. *J. Struct. Biol.* 130:323–338.